

# Materials for Quantum Technology



## PAPER

# Structural formation yield of GeV centers from implanted Ge in diamond

### OPEN ACCESS

RECEIVED  
9 November 2023

REVISED  
30 March 2024

ACCEPTED FOR PUBLICATION  
14 May 2024

PUBLISHED  
29 May 2024

Original content from this work may be used under the terms of the [Creative Commons Attribution 4.0 licence](#).

Any further distribution of this work must maintain attribution to the author(s) and the title of the work, journal citation and DOI.



Ulrich Wahl<sup>1,\*</sup> , João Guilherme Correia<sup>1</sup> , Ângelo Costa<sup>2</sup> , Afonso Lamelas<sup>3</sup> , Vítor Amaral<sup>3</sup> , Karl Johnston<sup>4</sup> , Goele Magchiels<sup>2</sup> , Shandirai Malven Tunhuma<sup>2</sup> , André Vantomme<sup>2</sup>  and Lino M C Pereira<sup>2</sup> 

<sup>1</sup> Centro de Ciências e Tecnologias Nucleares (C2TN), Departamento de Engenharia e Ciências Nucleares (DECN), Instituto Superior Técnico, Universidade de Lisboa, 2695-066 Bobadela LRS, Portugal

<sup>2</sup> KU Leuven, Quantum Solid State Physics, Leuven 3001, Belgium

<sup>3</sup> CICECO- Instituto de Materiais de Aveiro, Universidade de Aveiro, 3810-193 Aveiro, Portugal

<sup>4</sup> CERN-EP, 1211 Geneva 23, Switzerland

\* Author to whom any correspondence should be addressed.

E-mail: [uwahl@ctn.tecnico.ulisboa.pt](mailto:uwahl@ctn.tecnico.ulisboa.pt)

**Keywords:** diamond, germanium vacancy center, ion implantation, lattice location, emission channeling

Supplementary material for this article is available [online](#)

## Abstract

In order to study the structural formation yield of germanium-vacancy (GeV) centers from implanted Ge in diamond, we have investigated its lattice location by using the  $\beta^-$  emission channeling technique from the radioactive isotope  $^{75}\text{Ge}$  ( $t_{1/2} = 83$  min) produced at the ISOLDE/CERN facility.  $^{75}\text{Ge}$  was introduced via recoil implantation following 30 keV ion implantation of the precursor isotope  $^{75}\text{Ga}$  (126 s) with fluences around  $2 \times 10^{12}$ – $5 \times 10^{13}$   $\text{cm}^{-2}$ . While for room temperature implantation fractions around 20% were observed in split-vacancy configuration and 45% substitutional Ge, following implantation or annealing up to 900 °C, the split-vacancy fraction dropped to 6%–9% and the substitutional fraction reached 85%–96%. GeV complexes thus show a lower structural formation yield than other impurities, with substitutional Ge being the dominant configuration. Moreover, annealing or high-temperature implantation seem to favor the formation of substitutional Ge over GeV. Our results strongly suggest that GeV complexes are thermally unstable and transformed to substitutional Ge by capture of mobile carbon interstitials, which is likely to contribute to the difficulties in achieving high formation yields of these optically active centers.

## 1. Introduction

Group-IV vacancy centers in diamond are of high interest as spin-photon interfaces for a number of quantum applications, such as quantum information processing and quantum communication, with a particular focus on quantum networks [1–6]. Thanks to their symmetry properties (mirror-symmetric split-vacancy configuration), they exhibit no electric dipole moment, making their coherence less sensitive (compared to, e.g. nitrogen-vacancy centers NV) to electric noise originating from nearby material interfaces. This reduced sensitivity makes group-IV vacancy centers attractive for integration in nanophotonics. Among the group-IV vacancy centers, the  $\text{SiV}^-$  has been most extensively investigated. The realization of a quantum register [7] confirmed its compatibility with photonic nanodevices and it was also shown to exhibit a more efficient emission into the zero phonon line compared to NV centers [5]. However, its coherence time is limited at higher temperatures, requiring operation around 100 mK [5]. Heavier group IV impurities, with larger spin-orbit coupling, such as Ge, Sn and Pb, exhibit larger ground state splitting (50 GHz for  $\text{SiV}^-$ , 170 GHz for germanium-vacancy ( $\text{GeV}^-$ ), 850 GHz for  $\text{SnV}^-$ , 3.9–5.7 THz for  $\text{PbV}^-$  [5]) and hence allow for operation at higher temperatures. On the other hand, achieving effective control of the ground states is a challenging task due to the need for a corresponding microwave driver that matches the

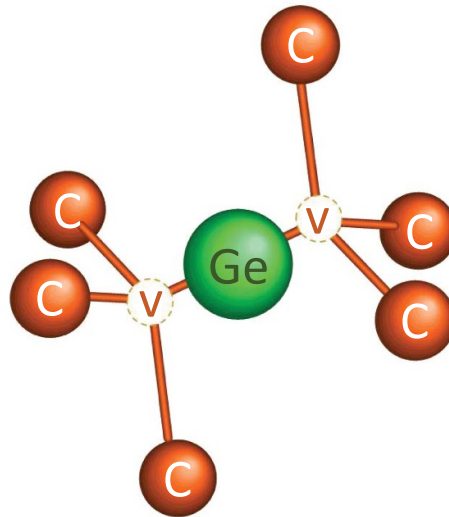


**Figure 1.** Atomic structure of the GeV complex in split-vacancy configuration: the Ge atom is located in an interstitial position midway between two adjacent vacancies V, which geometrically coincides with the so-called bond-center (BC) position in an undisturbed lattice.

larger ground state splitting (and even higher for  $\text{PbV}^-$  [5]).  $\text{GeV}^-$  centers can thus be expected to provide a good balance between higher operation temperature at less challenging driver frequencies.

The structure of group-IV vacancy centers in diamond can be pictured as the foreign atom occupying an interstitial site in the center of a double vacancy, the so-called split-vacancy configuration (figure 1) [1, 2, 4, 5], leading to a group-IV lattice site that is geometrically identical to the so-called ‘bond-center (BC) position’ in an ideal diamond crystal. Note that in this manuscript we use the term ‘BC site’ as it is used within the ion beam analysis community, i.e. simply indicating this specific geometric position in the lattice without regards as to whether it represents the center of a chemical bond.

The negatively charged  $\text{GeV}^-$  defect was discovered in 2015 by Iwasaki *et al* [8] who produced it via ion implantation, followed by annealing at temperatures  $>800^\circ\text{C}$ , as well as by means of doping during chemical vapor deposition (CVD) growth; at about the same time high-pressure synthesis of GeV-doped microdiamonds was reported [9, 10]. While doping during growth is thus feasible, creation by ion implantation offers various advantages regarding defect positioning and concentration control. However, the reliable and reproducible fabrication of  $\text{GeV}^-$  centers has remained a key challenge for practical development of GeV-based devices. In that respect, the formation yield of optically active  $\text{GeV}^-$  following ion implantation was reported to be 0.4%–0.7% [11] and 1.9% [3], hence tentatively lower than in the case of  $\text{SiV}^-$  (0.5%–1% [12], 0.5%–6% [13, 14],  $\sim 1\%$ –3% [15],  $\sim 2\%$  [16],  $\sim 2.5\%$  [17], 2.5%–3.75% [18], 2.98% [19], 3.2% [3], 5% [20], 15% [21]) or  $\text{SnV}^-$  ( $\sim 0.7\%$  [22],  $>1\%$  [23], 0.4%–3% [24], 1%–4% [25, 26],  $\sim 2.5\%$  [17],  $\sim 5\%$  [27], 60% [28]). GeV centers have also been produced by means of recoil implantation via Xe-irradiation of thin Ge films deposited on diamond, followed by  $950^\circ\text{C}$  annealing [29]. In this case, the formation yield of optically active  $\text{GeV}^-$  was reported at maximum  $\sim 0.15\%$  with respect to each irradiated Xe ion, higher than in the case of Sn recoil implantation (0.04%) [29].

It should be pointed out that there is a fundamental difference between the concepts of ‘structural formation yield’ and ‘optically active formation yield’. While structural formation yield describes the relative amount of (implanted) Ge atoms in GeV split-vacancy configuration, optically active formation yield refers to the fraction of (implanted) Ge atoms that actually produce a  $\text{GeV}^-$  optical signal. While the structural formation yield needs to be assessed by methods that are sensitive to the structure of defects, optically active formation yields are determined by counting the number of  $\text{GeV}^-$  emitters in a certain area of the sample and putting it in relation to the implanted fluence. Since it is possible that a Ge atom is incorporated in split-vacancy configuration but is actually not optically active because the corresponding GeV complex is in a ‘dark state’, e.g. not in the required negative charge state, or optical activity is quenched due to the presence of other defects, it is expected that the structural formation yield will generally be higher than the optically active one. This has been found to be the case for the SnV [30] and the MgV [31] defects, where structural formation yields around 30%–40% were reported, an order of magnitude higher than optically active SnV $^-$  and MgV $^-$ .

While a considerable number of publications have addressed the theoretical aspects of the GeV complex with regards to its atomic structure, electronic level scheme and optical transitions [8, 10, 32–42],

calculations of its energetics of formation and stability are scarcer [32, 37, 39, 42]. Reference [32] predicted that the energy of formation of simple substitutional  $\text{Ge}_s$ ,  $E_f(\text{Ge}_s)$ , is 1.1 eV lower than  $E_f(\text{GeV})$  for the GeV complex in split-vacancy configuration, hence that  $\text{Ge}_s$  should be more stable than GeV. More detailed calculations in [39] addressed the formation energy as a function of the position of the Fermi level and corresponding GeV charge state, arriving at the result that the formation energy for neutral substitutional  $\text{Ge}_s^0$  is 1.8 eV lower than for neutral  $\text{GeV}^0$ , and that only for Fermi level positions above 3.5 eV, i.e. in *n*-doped diamond, negatively charged  $\text{GeV}^-$  should be energetically more favorable than simple substitutional  $\text{Ge}_s$ .

The issue of group IV elements forming higher order vacancy complexes than GeV, such as  $\text{GeV}_2$  or  $\text{GeV}_3$ , has not been addressed systematically in the literature. Reference [39] predicts the energy of formation of  $\text{GeV}_2$  to be somewhat higher than for GeV, with a structure consisting of 'a GeV defect in the split-vacancy position located near a second vacancy'. Reference [37] discusses the energetics of the interaction of group IV–vacancy complexes with additional carbon vacancies  $V_C$  and shows a  $\text{GeV}-V_C$  complex where the Ge atom remains on its BC site, with an additional vacancy attached to it.

In any case, ion implantation happens far from thermodynamic equilibrium since through radiation damage large amounts of vacancies are created that exceed by far the vacancy concentrations produced by annealing or doping during growth at high temperatures. Consequently, since the energy required to create the vacancies involved in vacancy-related complexes has been provided by the kinetic energy of the implanted ions, it is therefore not obvious that impurities preferentially assume configurations that have the lowest thermodynamic formation energy. The cohesive energy of diamond, i.e. the energy that binds a carbon atom to the crystal, is 7.37 eV [43]. However, in ion implantation, the displacement energy threshold  $E_d$ , i.e. the energy that needs to be transferred to a carbon atom so that it travels far enough to not recombine immediately with its vacancy, has been found to be higher, in the range 35–80 eV (often  $\sim 45$  eV is assumed) [44]. Accordingly, 'Stopping and Range of Ions in Matter' (SRIM) simulations [45] with  $E_d = 45$  eV predict, e.g. that about 200 vacancies and interstitials are created following 30 keV implantation of Ge into diamond.

As we will show, our experimental results strongly suggest that simple substitutional  $\text{Ge}_s$  is the preferred configuration formed upon ion implantation in diamond, despite the large numbers of vacancies created in the process, with GeV produced to a smaller extent as well, but being thermally unstable and thus subject to significant reduction during thermal annealing. This suggests a general drawback for the efficient production of this color center, not only by ion implantation but possibly also by means of doping during growth techniques, where less vacancies are available for the formation of this center than in ion implantation.

## 2. Experimental

Currently, the only experimental technique which can assess the lattice position occupied by implanted impurities in a fluence range that is relevant for quantum applications in diamond, is the emission channeling (EC) method using radioactive isotopes [46, 47], which allows to accurately examine the lattice sites of impurities implanted at fluences as low as  $10^{11} \text{ cm}^{-2}$ . The general principle of the EC technique is that charged particles emitted during the decay of radioactive isotopes (in our case  $\beta^-$  particles) experience channeling and blocking effects on their way out of the single crystal. This leads to anisotropic angular emission of decay particles in the vicinity of major crystallographic axes and planes, which can be detected using a position-sensitive detector (PSD) [48] placed at an appropriate distance from the sample. The experimental setup used for that purpose is as described in [49].

Our experiments were performed at the ISOLDE/CERN on-line isotope separator facility [50]. Since ISOLDE cannot deliver radioactive Ge ion beams, we resorted to implanting the short-lived precursor isotope  $^{75}\text{Ga}$  ( $t_{1/2} = 126$  s), which decays into  $^{75}\text{Ge}$  by means of  $\beta^-$  decay ( $\beta^-$  endpoint energy 3300 keV, mean energy 1392 keV). During this decay, the  $^{75}\text{Ge}$  daughter nuclei receive recoils of up to 102 eV, which considerably exceeds the cohesive energy of diamond (7.58 eV) and thus causes them to be re-implanted, and, since the maximum recoil also exceeds the displacement energy threshold of  $\sim 45$  eV, possibly even creates some additional vacancies. The relevant probe atom  $^{75}\text{Ge}$  (82.87 min) decays into stable  $^{75}\text{As}$ , also via  $\beta^-$  decay ( $\beta^-$  endpoint energy 1176 keV, mean energy 419.5 keV). The precursor isotope  $^{75}\text{Ga}$  was produced by means of bombarding a heated  $\text{UC}_2$  target with 1.4 GeV protons, followed by out diffusion, selective ionization of Ga through a resonant laser ion source [51], and electromagnetic mass separation.

The samples were  $\langle 100 \rangle$  oriented single crystals from ElementSix, termed 'SC plate CVD', of size  $3.0 \times 3.0 \times 0.25 \text{ mm}^3$ , with nitrogen concentrations  $[N] < 1$  ppm. Two samples were studied, roughly differing by a factor of 10 in the implanted fluence: the lower fluence sample with  $\sim 2 \times 10^{12} \text{ cm}^{-2}$  per implantation step and a single beam spot for implantation temperatures of room temperature (RT, 30 °C), 300 °C, 600 °C, and 900 °C (the highest temperature that can be reached in our setup); the higher fluence sample with  $\sim 2 \times 10^{13} \text{ cm}^{-2}$  per implantation step and 3 different beam spots for implantation at RT,

300 °C, and 600 °C, and annealing temperatures of 300 °C, 600 °C, and 900 °C (10 min, vacuum better than  $10^{-5}$  mbar).

Implantations were performed with 30 keV energy into a 1 mm diameter beam spot, with a mean current of 7 pA ( $4.4 \times 10^7$  particles  $s^{-1}$ ) in case of the lower-fluence sample, and 15 pA ( $9.4 \times 10^7$  particles  $s^{-1}$ ) in case of the higher-fluence sample. All implantations occurred under an angle of  $17^\circ$  from the  $\langle 100 \rangle$  surface normal of the crystal (mean range 149 Å, straggling 36 Å from SRIM [45]), which faced the PSD, thus allowing to measure the  $\langle 100 \rangle$  EC effects resulting from the precursor isotope  $^{75}\text{Ga}$  during implantation. Following each  $^{75}\text{Ga}$  implantation, a waiting time of 10 min (roughly 5 half lives) assured that contributions from the precursor isotope to the first measured pattern of  $^{75}\text{Ge}$  were at maximum a few percent of events and completely negligible for subsequent measurements. The same waiting time after implantation was applied before performing sample annealing. A more detailed description of implantation sequences can be found in the supplementary material [52].

In order to detect the emitted  $\beta^-$  particles, we used a  $22 \times 22$  pixel Si pad detector [48] of pixel size 1.3 mm which was placed at 60 cm distance from the sample, thus achieving angular resolution of  $\sim 0.05^\circ$ . The major occupied lattice sites were identified by least squares fitting [53] the experimentally observed emission patterns by linear combinations of theoretical patterns calculated for substitutional (S) and bond-centered (BC) positions. Theoretical emission patterns for various lattice sites were simulated using the ‘many beam’ approach [47, 48], and more details can be found in the supplementary material [52].

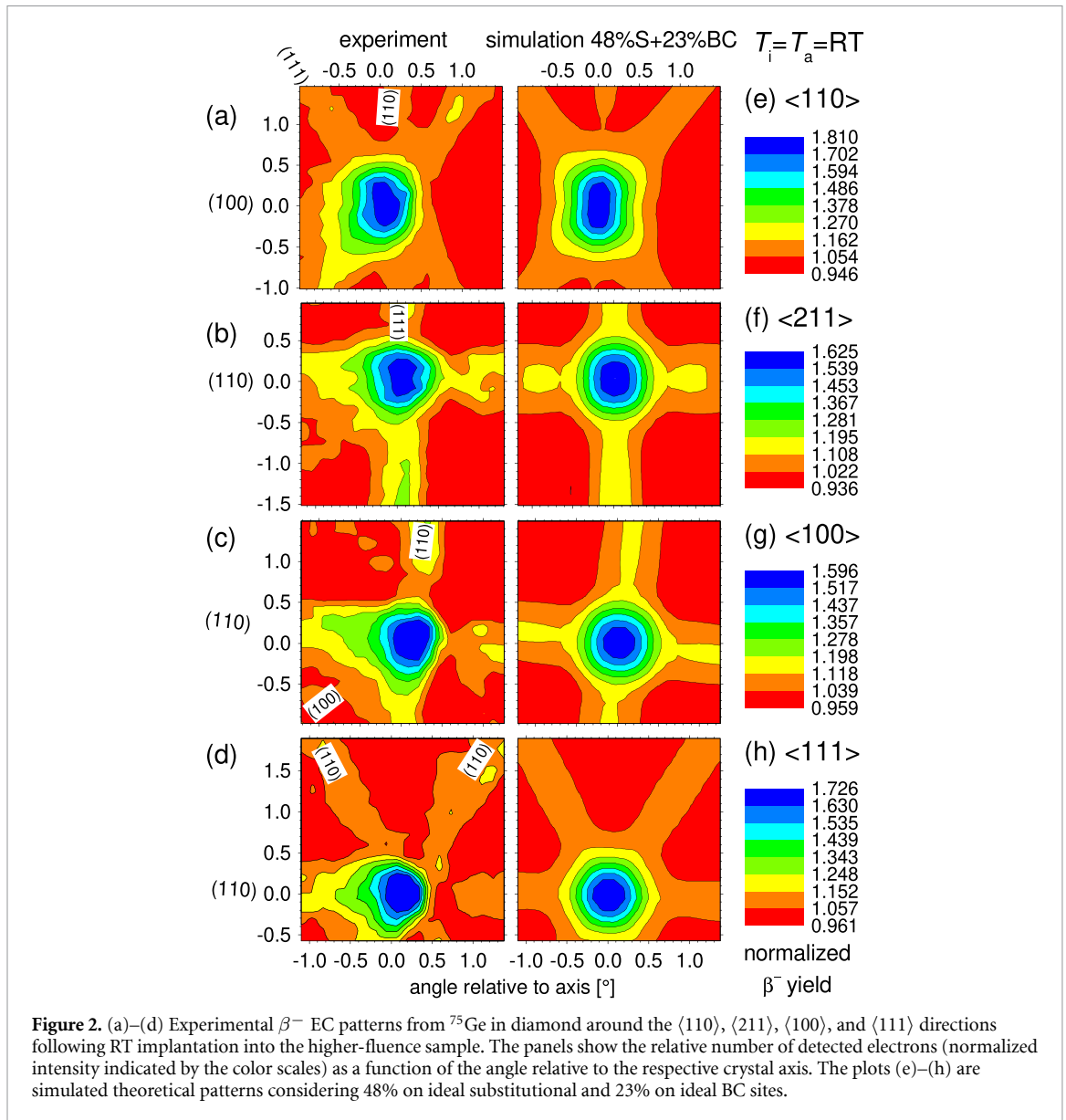
The measurement of electron EC effects is always subject to background from two sources [30, 53]: a) electrons that are backscattered from inside the sample or from the walls of the vacuum chamber towards the detector, b) the background of gamma radiation caused in the detector by the gamma emission from the sample itself and radioisotopes in the vicinity, including the ISOLDE targets, which are about 10 m meters away and shielded, while contributions from cosmic radiation are negligible for studies of high-activity samples like in this work. Contribution (a) was estimated using GEANT4 [54] Monte Carlo simulations of electron trajectories, taking into account the geometry and construction materials of our experimental setup. Contribution (b) was assessed by closing a shutter valve in front of the detector, which stops all electrons but lets pass most of the gamma radiation from the sample and the vicinity. Background contributions were accounted for by multiplying fitted lattice site fractions with correction factors, which were estimated to be 1.80–1.85 for the measurements during the  $^{75}\text{Ga}$  implantations and 1.75–2.16 for  $^{75}\text{Ge}$ , the latter depending on sample activity vs background. Due to the method of estimating the background, there is a *relative* error in  $\sim 10\%$  in the sum of the fractions of emitter atoms on all types of lattice sites. This error means that also sum fractions can be reached that are somewhat larger than 100%. For specific site fractions, a *relative* error of 10% means, e.g. that an assigned fraction of 20% is subject to an error of  $\pm 2\%$  due to background correction.

### 3. Results

#### 3.1. Lattice location of $^{75}\text{Ge}$

Figure 2 panels (a)–(d) show the experimental  $\beta^-$  EC patterns from  $^{75}\text{Ge}$  recoil-implanted from  $^{75}\text{Ga}$  decay at RT in the higher-fluence sample, in the vicinity of the  $\langle 110 \rangle$ ,  $\langle 211 \rangle$ ,  $\langle 100 \rangle$  and  $\langle 111 \rangle$  crystallographic directions. The normalized  $\beta^-$  emission yields are indicated by the color scales and the channeling anisotropy is highest along the axial directions near the center of the patterns, with major planes (111) and (110) also showing pronounced channeling effects, while anisotropy effects from (100) planes are basically absent. The corresponding patterns for RT implantation followed by annealing at 900 °C can be found in figures 3(a)–(d), those for implantation at 900 °C in figures 4(a)–(d), while figure S1 in the supplementary material [52] summarizes the channeling anisotropy values of the axial effects as a function of annealing and/or implantation temperature for both samples. These experimental patterns are available via reference [55]. We first notice the very pronounced anisotropies of the normalized  $\beta^-$  yield in all of the patterns (anisotropies in the range 1.6–2.6, compared to 1.3–2.0 for  $^{121}\text{Sn}$  [30] or 1.1–1.3 for  $^{27}\text{Mg}$  [31]). Such strong channeling effects are usually only measured when the major part of the probe atoms occupies substitutional sites. As a second observation we point out that for all crystallographic directions there is a pronounced increase in channeling effects with increasing implantation or annealing temperature. This usually indicates changes in the lattice site configuration of the probe atoms or the annealing of implantation damage.

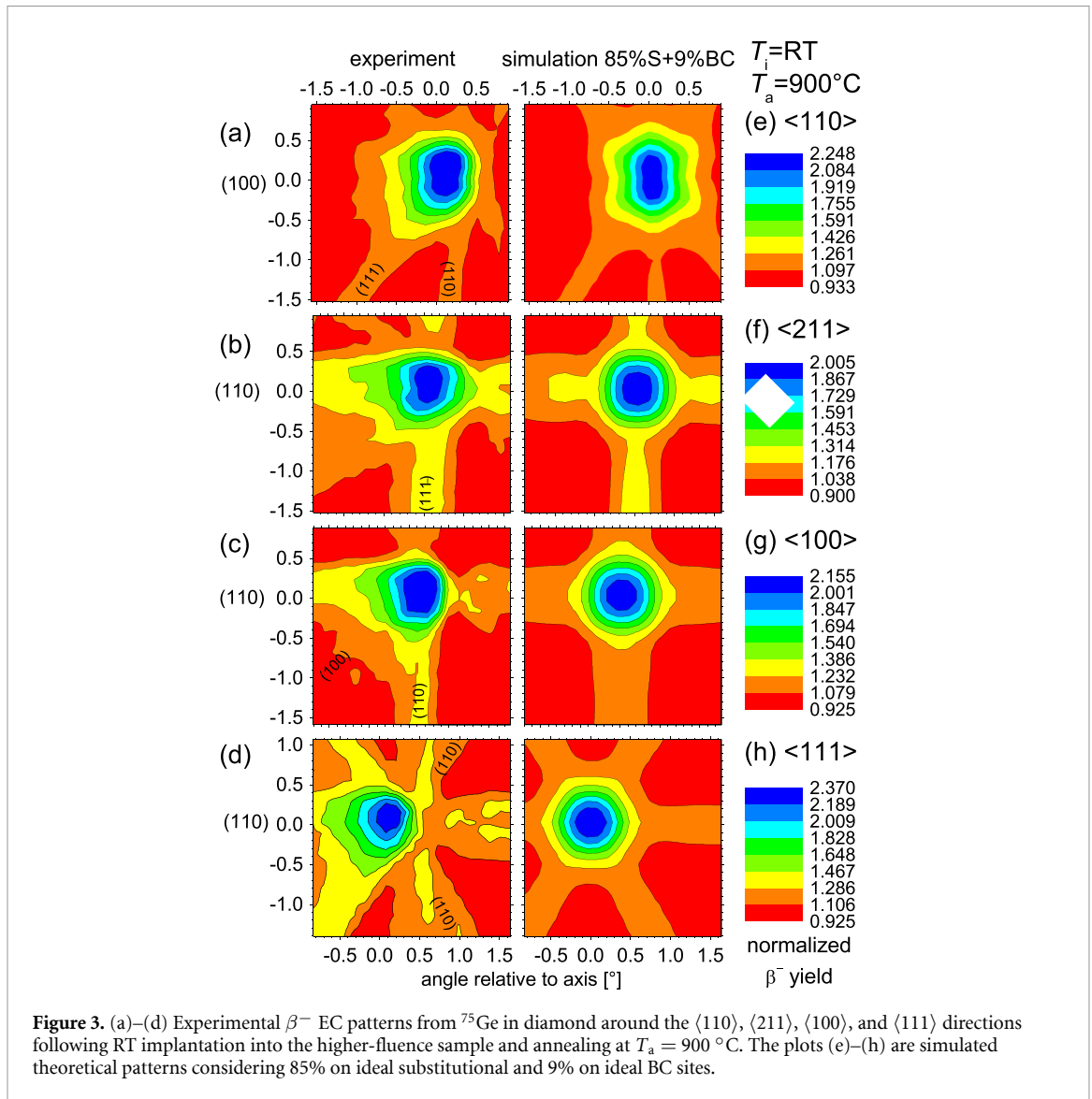
In order to *quantitatively* evaluate the possible fractions of  $^{75}\text{Ge}$  on different lattice sites, the experimental patterns were then fitted by linear combinations of theoretically calculated patterns for up to two different lattice sites. The fit procedure [53] allows to extract the fractions of emitter atoms on the different lattice sites that correspond to the experimental results. When considering only single sites in the fit, the best fits were always for the substitutional site, as was already suggested by the large anisotropies of the patterns. When in



addition to the substitutional position a second lattice site was allowed, the BC site provided improvements in chi square fit quality of up to 8% for  $\langle 100 \rangle$  patterns, 2% for  $\langle 110 \rangle$  and  $\langle 211 \rangle$  in comparison to one-site fits with S sites only.

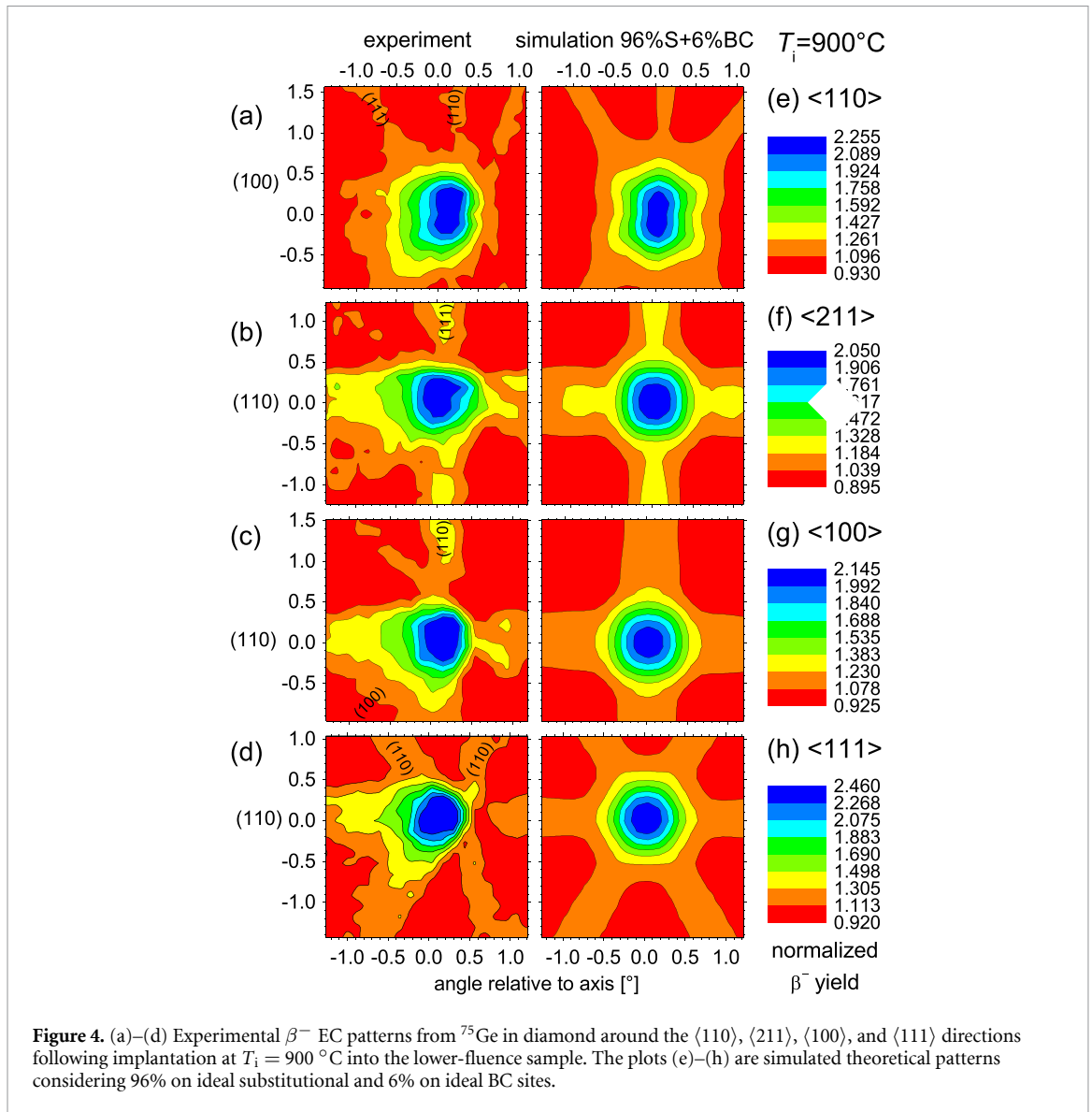
The theoretical patterns corresponding to  $^{75}\text{Ge}$  on either S or BC sites are shown in figure 5. S sites cause very strong channeling effects along all axial directions, as well as along the major planes (111) and (110), while planar (100) channeling effects are rather weak so that they are not visible in the color scale contrast of the patterns. For BC sites, which are sites of lower crystal symmetry, the maximum axial anisotropies for all four directions are much less pronounced. In fact, for BC sites the strongest channeling features are now the (111) planes, with much weaker channeling remaining along (110) planes, while (100) planes have changed to blocking effects, as has the axial  $\langle 100 \rangle$  direction. The blocking effects are understandable from geometric arguments when looking at the projections of the lattice sites along the various axial and planar directions (figure 6): BC sites are always located in the potential maximum in between atomic  $\langle 100 \rangle$  axes or (100) planes, which causes electron trajectories to be deflected when emitted from these sites. On the other hand, the strong (111) planar channeling from BC sites is not obvious from geometric arguments but a characteristic peculiarity of the diamond structure, where (111) planes occur in close pairs of atomic planes. Three out of four possible projections of BC sites are located in the center of such (111) pairs of planes (best visible for the  $\langle 211 \rangle$  projection in figure 6), where emitted electrons are still bound to the atomic potential resulting from the superposition of the pair of planes, which causes a strong channeling effect. Note that the theoretical patterns in figure 5 are represented without contributions from background. This means that the *calculated* anisotropies of channeling and blocking effects are considerably more pronounced than what can





be measured in the experiment. Flat background contributions of 43%–54% for patterns from  $^{75}\text{Ge}$  mean that the maximum measurable anisotropies are a factor of  $\sim 2$  below the calculated ones, e.g. for 100% of  $^{75}\text{Ge}$  atoms on substitutional sites, the expected maximum normalized yield resulting from the  $\langle 110 \rangle$  pattern in figure 5(a) is only  $(4.120 - 1)/2 + 1 = 2.56$ , for the other directions, values around 2.00 for  $\langle 211 \rangle$ , 2.18 for  $\langle 100 \rangle$ , and 2.23 for  $\langle 111 \rangle$  are expected. The experimentally observed maximum normalized yields following  $900^\circ\text{C}$  annealing (figure 3) or implantation (figure 4) match these values rather well, e.g., from figure 3: 2.26 for  $\langle 110 \rangle$ , 2.05 for  $\langle 211 \rangle$ , 2.15 for  $\langle 100 \rangle$ , and 2.46 for  $\langle 111 \rangle$ , which indicates, even without performing a detailed fit procedure, that close to 100% of  $^{75}\text{Ge}$  emitter atoms must occupy substitutional sites.

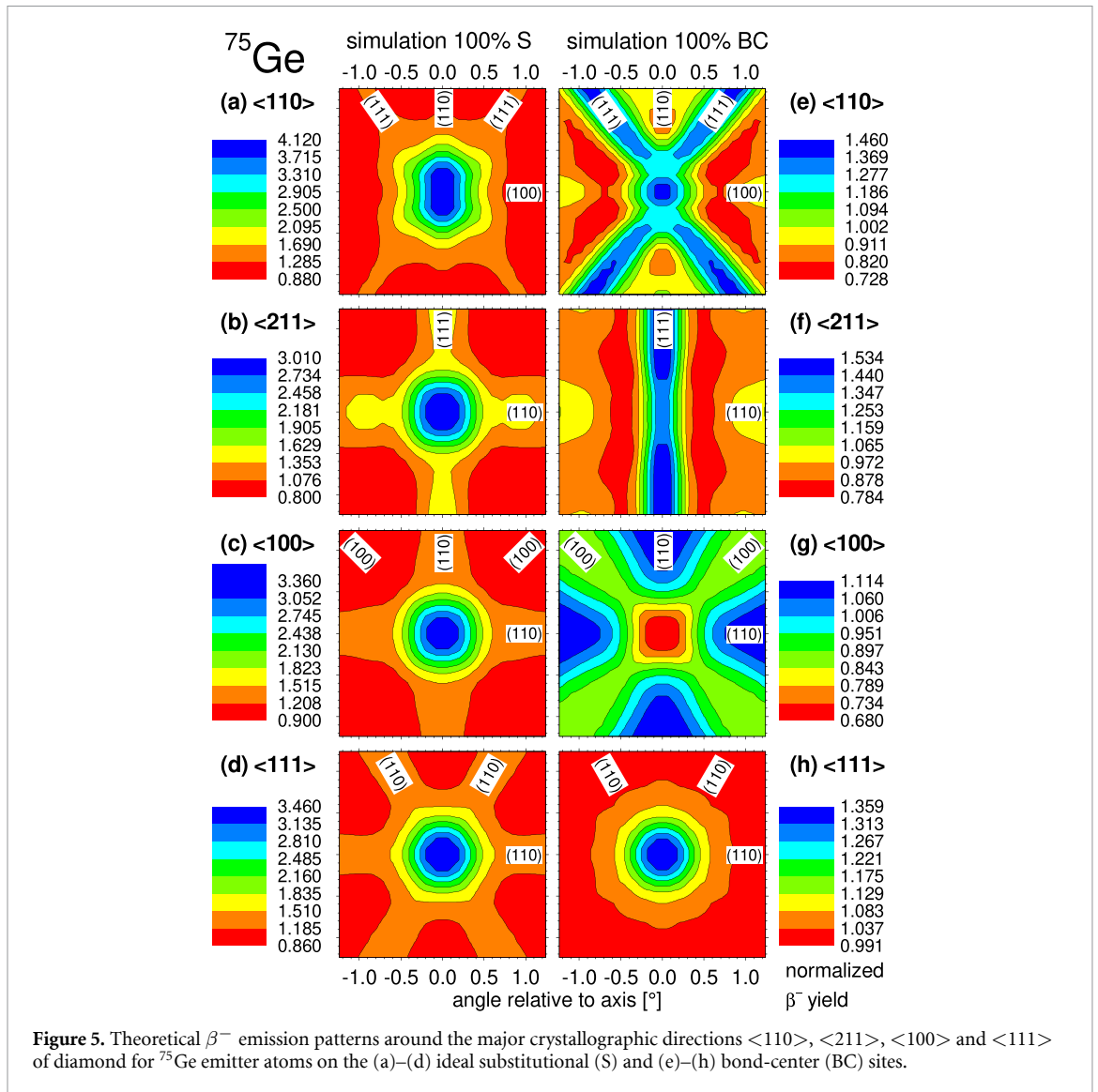
The resulting best fits of theoretical patterns for  $\langle 110 \rangle$ ,  $\langle 211 \rangle$  and  $\langle 100 \rangle$  directions are shown in panels (e)–(g), respectively, of figures 2–4. As was previously remarked [30],  $\langle 111 \rangle$  patterns are not suitable for a discrimination of S and BC positions, since their structure is too similar for these two lattice sites (figures 5(d) and (h)), which makes the fit results unstable. The theoretical patterns in panels (h) of figures 2–4 are hence not fit results but calculated using the fractions derived from the other directions. The fitted  $^{75}\text{Ge}$  fractions on S and BC sites and their sum are compiled in figure 7 for the various implantation conditions of the lower-fluence (panel (a)) and higher-fluence (panel (b)) samples. We first note that the sum of S and BC fractions increases from 60%–70% for RT implantation up to 95%–105% following  $900^\circ\text{C}$  implantation or annealing. Sum fractions smaller than 100% mean that there is a flat contribution without anisotropy to the channeling patterns, which in the channeling community is usually called the ‘random’ fraction. This may result from implanted probe atoms which are located on lattice sites that do not cause measurable channeling effects or are in a highly defective environment, but also from flat background that



was not properly corrected. In that respect, the procedures for background correction described above, lead to uncertainties of the order of 10% in the random vs. sum fractions. Therefore, sum fractions larger than 100% are likely to result from an overestimation of the contribution of background to the measurement. In any case, an increase in the sum fractions suggests effects of local damage annealing in the samples, which is accompanied by the increased incorporation of  $^{75}\text{Ge}$  atoms in well-defined sites. However, since the sum fraction is not correlated with the implanted fluence, it indicates that this is still damage annealing inside isolated collision cascades. The second effect of annealing or implantation at elevated temperatures is the reduction of the fraction of  $^{75}\text{Ge}$  atoms on BC sites, which seem to change their lattice position to S sites. It is worthwhile mentioning that no significant differences in fractions were observed in between implantation temperature and post-implantation annealing at the same temperature. Thus, in all cases, the observed BC fractions were highest for RT implantations, around 18%–22%, with practically no difference between lower- and higher-fluence samples. For higher implantation or annealing temperatures, the BC fractions are significantly reduced, around 6%–9% for  $900^\circ\text{C}$ , while the substitutional fraction grows to around 85%–96%.

### 3.2. Lattice location of the precursor isotope $^{75}\text{Ga}$

Information on the lattice location of the precursor isotope  $^{75}\text{Ga}$  could be extracted from the corresponding  $\langle 100 \rangle$  patterns acquired during implantation, which are shown for four of the  $^{75}\text{Ga}$  implantations in figures 8(a)–(d). Note that other directions could not be measured since the orientation of the sample during implantation needed to be kept fixed in order to assure a well-defined beam spot with the same depth profiles for all implantation conditions. Moreover, channeling patterns were not measured during all



implantations, since the periods of implantation were also taken advantage of for background measurements with the detector shielded. The EC effects from  $^{75}\text{Ga}$  are all considerably narrower than from  $^{75}\text{Ge}$ . This is not a consequence of largely different lattice site contributions, but due to the fact that the angular width of channeling effects scales approximately proportional to the inverse of the square root of the particle energy, which is higher for the short-lived  $^{75}\text{Ga}$  than for the longer-lived  $^{75}\text{Ge}$  (mean  $\beta^-$  energies 1392 keV vs. 419.5 keV). The second observation is that the maximum anisotropy increases significantly with implantation temperature, cf also figure S2 in supplementary material [52], from 1.54–1.60 at 30 °C to 2.06 at 600 °C, which indicates annealing of implantation damage or possible site changes of  $^{75}\text{Ga}$ , similar to the case of the daughter isotope  $^{75}\text{Ge}$ .

The S and BC fractions for  $^{75}\text{Ga}$  derived from the fits of the  $\langle 100 \rangle$  patterns, where these were measured during implantation, are shown in figure 9. We notice that the BC fractions of  $^{75}\text{Ga}$  tend to be higher than for  $^{75}\text{Ge}$ , 30% vs. 20% for RT implantation, while the substitutional fractions are lower. Thus, the split-vacancy configuration is produced in larger amounts in the case of Ga, in fact at RT practically as frequently as the substitutional incorporation. Another striking difference, is that in the case of  $^{75}\text{Ga}$  at an implantation temperature of 600 °C the BC fraction is only slightly lower than for 30 °C or 300 °C, in contrast to  $^{75}\text{Ge}$ , where it decreased already considerably at this temperature. This indicates that the split-vacancy configuration for Ga, which is associated with the BC fraction, does not suffer from thermal instability to the same extent as in the case of Ge, in line with theoretical predictions that GaV is thermally more stable than simple substitutional Ga<sub>S</sub> [32, 56]. We would like to point out that from the viewpoint of structural formation yield and thermal stability, this raises good prospects to create GaV defects by means of ion implantation, predicted as promising spin-1 color centers in their negative charge state GaV<sup>-</sup> [56, 57].



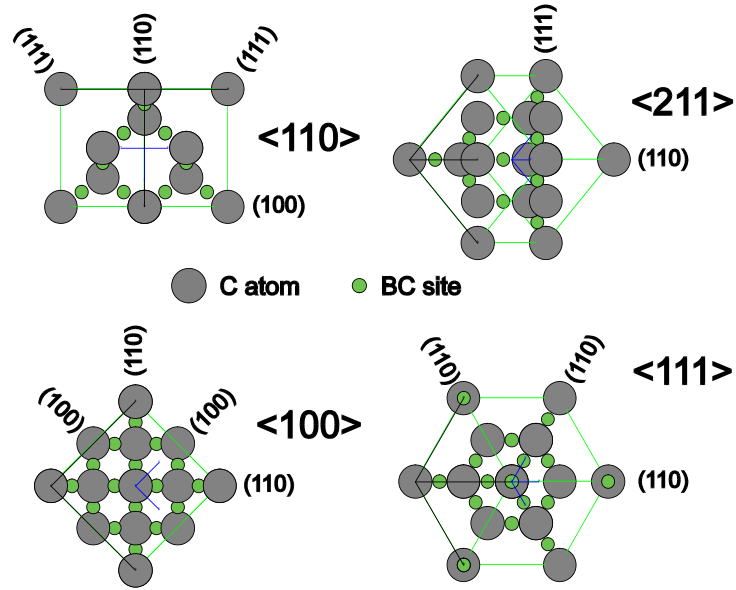


**Figure 6.** Schematic atomic projections along the major crystallographic directions of a diamond unit cell. The positions of all bond-center (BC) sites within the unit cell are shown as small green circles.

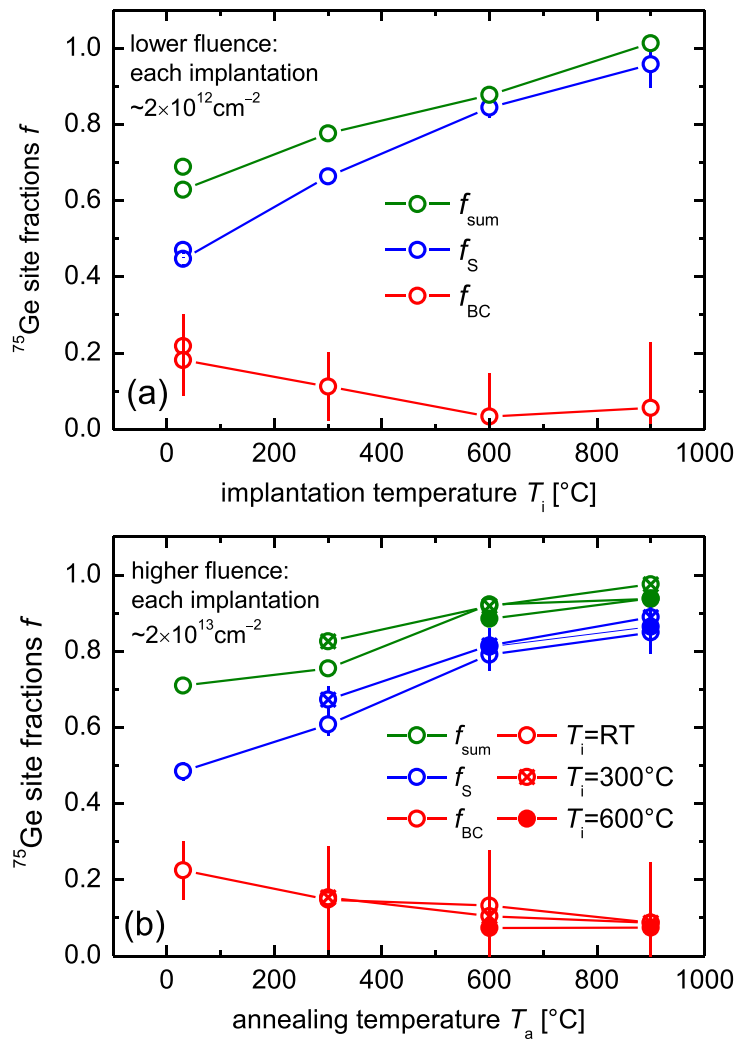
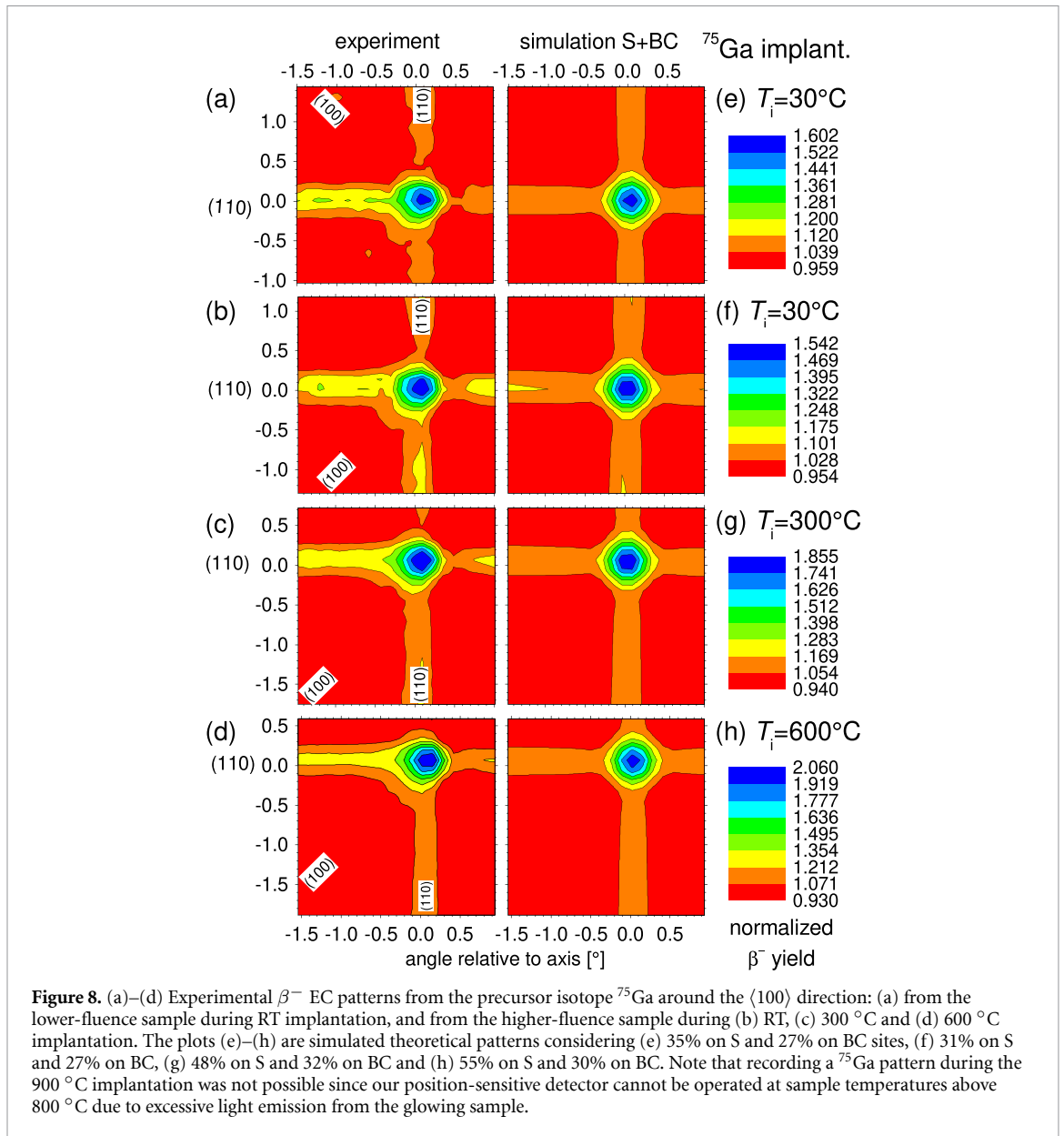


**Figure 7.** <sup>75</sup>Ge site fractions on substitutional ( $f_S$ ) and bond-center ( $f_{BC}$ ) sites and their sum ( $f_{sum}$ ) as a function of annealing and implantation temperatures  $T_a$  and  $T_i$  in the lower-fluence (a) and higher-fluence (b) samples.



#### 4. Discussion

While the 20% fraction of Ge found in bond-center sites following room temperature implantation is a factor of  $\sim 2$  smaller than, e.g. in the case of Sn (40%) [30] or Mg (42%) [31], it shows that a significant amount of GeV defects are created in the as-implanted state. However, in the case of Sn (32%) [30] or Mg (30%) [31] much higher fractions survive 800 °C–900 °C annealing or implantation than in the case of Ge (6%–9%). We note, though, that the surviving BC fraction of  $\sim 6\%$  is still a factor of 3–10 higher than the reported formation yields of *optically active* GeV $^-$  (0.4%–0.7% [11], 1.9% [3]).

It is frequently stated in the literature, e.g. [1, 4, 8, 17, 24, 25, 28, 58], that thermal annealing with the aim of driving vacancies towards the implanted impurity would be an essential step in the formation mechanism of impurity-vacancy complexes in diamond. While this concept has proven valuable in what concerns formation of the nitrogen-vacancy complex, it is clearly not correct for the cases of Sn, Mg, Ge, and Ga since it was shown already that both SnV [30] and MgV [31] complexes are quite obviously already formed in significant amounts in the RT as-implanted state, as is also shown for GeV and GaV in this work. Since thermal annealing in all these cases actually reduced the amount of split-vacancy complexes, we conclude that it is required in order to restore or modify the crystal environment so that luminescence from the color centers can be excited and/or observed, possibly to assure the required negative charge state of the split-vacancy complexes, but not to increase their *structural* formation yields. The structural formation happens already rather efficiently due to the thermal spike following implantation, as mentioned below.

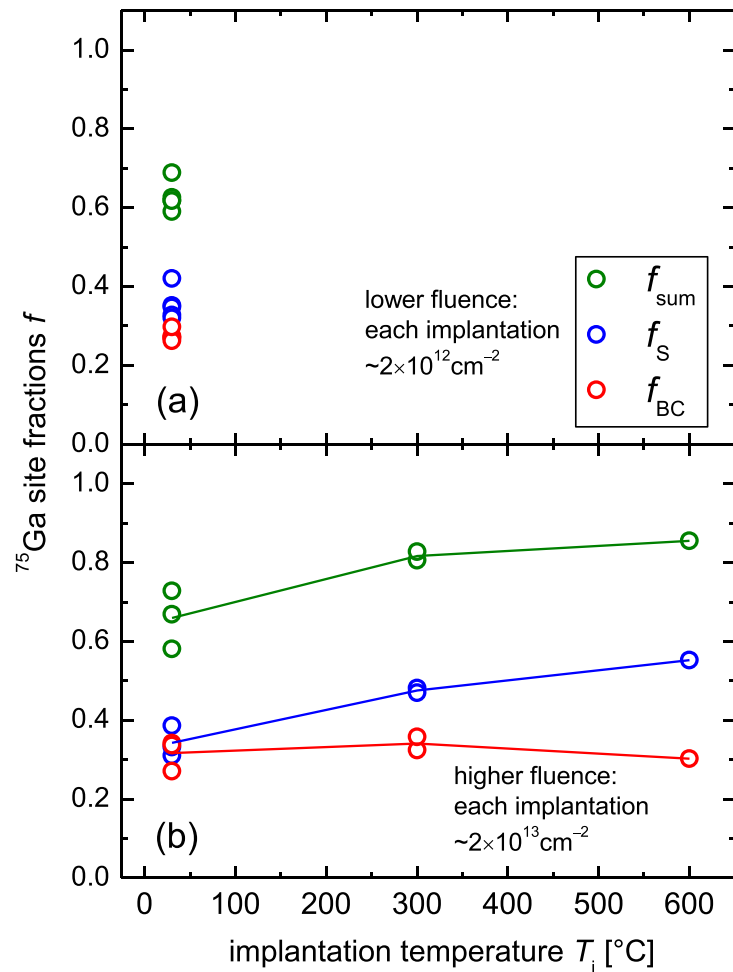


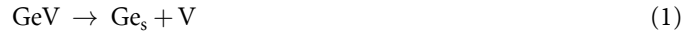
**Figure 9.**  $^{75}\text{Ga}$  site fractions on substitutional ( $f_S$ ) and bond-center ( $f_{BC}$ ) sites and the sum of both ( $f_{\text{sum}}$ ) for implantation temperatures of (a) 30 °C in the lower-fluence, and (b) 30 °C, 300 °C and 600 °C in the higher-fluence sample.

A somewhat surprising fact is that, for the fluence range and temperatures studied in this work, it seems to make hardly any difference whether the diamonds are implanted at a specific temperature or post-implant annealed at the same temperature. This behavior is unexpected, since an increase in implantation temperature is usually much more effective in stimulating radiation damage annealing effects than a post-implant anneal at the same temperature. This indicates that the lattice sites of  $^{75}\text{Ge}$ , which are in fact occupied following recoil implantation, when the thermal spike from  $^{75}\text{Ga}$  has died out already, are not very sensitive to the overall vacancy concentrations in the sample.

Due to the particular introduction method of Ge used in the current study, i.e. via implantation of the  $^{75}\text{Ga}$  precursor isotopes and recoil implantation of  $^{75}\text{Ge}$ , the formation yields of GeV in our case can be different compared to the direct implantation of Ge. Here one should take into account the fact that recoil implanted  $^{75}\text{Ge}$  starts from lattice sites that are specific for  $^{75}\text{Ga}$  atoms and, since recoil momentum is shared between the nucleus and the emitted  $\beta^-$  and anti-neutrino particles,  $^{75}\text{Ge}$  recoil energies have a distribution up to the maximum value of 102 eV. It is therefore conceivable that for some  $^{75}\text{Ga}$  decays the recoil is too small to result in a change of lattice site of the  $^{75}\text{Ge}$  daughter atom. Moreover, recoil implantation of each  $^{75}\text{Ge}$  atom introduces roughly a factor 500 less kinetic energy into the sample than the original implantation of the precursor  $^{75}\text{Ga}$  ion. This energy is subsequently thermalized in what is often called a ‘thermal spike’, meaning that recoil implanted atoms have to find their lattice site with much less thermal spike energy available in the crystal. However, our experiments also monitor the *thermal stability* of the split-vacancy configuration against annealing, and this should be the same irrespective of its method of production, i.e. direct vs recoil implantation of Ge. In that respect, the fact that the GeV fraction is already significantly reduced following annealing at 300 °C and reaches less than 10% after 900 °C annealing, in combination with an increase in the substitutional fraction, suggests that GeV is thermally unstable in comparison to simple substitutional  $\text{Ge}_s$ .

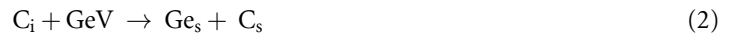
Next we would like to address possible pathways that may be responsible for the conversion of GeV to simple substitutional Ge<sub>s</sub>. As we will see below, they involve the migration of interstitial carbon C<sub>i</sub> or the vacancy V. In that respect, it seems generally accepted that vacancies and interstitials in diamond migrate in their neutral charge state with activation energies of  $E_m(V) = 2.3$  eV [59, 60] and  $E_m(C_i) = 1.6$  eV [60–62], respectively. The required temperature for interstitial migration ( $\sim 400$  °C) is thus quite lower than for vacancy migration ( $\sim 700$  °C) [63]. One may then consider two basic reaction mechanisms for the conversion of GeV to Ge<sub>s</sub>:

the dissociation reaction



meaning that one vacancy is released from the GeV in split-vacancy configuration and then travels at least a short distance away from the remaining substitutional Ge<sub>s</sub> in order to prevent re-formation of the split-vacancy configuration;

the capture reaction



meaning that an interstitial C<sub>i</sub> migrates to the GeV defect, fills up one carbon vacancy and thus pushes the Ge atom into a substitutional position. Reaction (1) is associated with an activation energy for dissociation  $E_a = E_b(\text{GeV}) + E_m(V)$  [31] that is the sum of the binding energy  $E_b(\text{GeV})$  of the complex, which has been predicted in [31] as being  $E_b(\text{GeV}^-) = 6.0$  eV,  $E_b(\text{GeV}^0) = 4.9$  eV and  $E_b(\text{GeV}^+) = 7.5$  eV for various charge states, plus the migration energy of the vacancy  $E_m(V)$ , thus at least  $E_a > 7.2$  eV. Note that overcoming such high activation energies would require temperatures above 2000 °C.

On the other hand, reaction (2) only requires to overcome the migration energy  $E_m(C_i)$  of the interstitial C<sub>i</sub> as reaction barrier, since removal of an interstitial C<sub>i</sub> from the lattice and filling up one of the vacancies of GeV is associated with an energy gain. The fact that we observed significant conversion of GeV to Ge<sub>s</sub> already starting at 300 °C, hence suggests this process to be related to the short-range migration of C<sub>i</sub> interstitials created by the implantation.

In this scenario, defining the thermal stability of GeV in diamond becomes a more nuanced matter. As long as there is a high concentration of C<sub>i</sub> (at least in the vicinity of the implanted Ge atom) the GeV defect has a low thermal stability, associated with the tendency for C<sub>i</sub> to diffuse and combine with the V in the GeV defect in reaction (2). However, once all the C<sub>i</sub> defects have essentially annealed out, the remaining GeV centers that survived the processing up to that point have now a much larger thermal stability, since only reaction (1) is allowed, which according to the theoretical predictions should not take place below 2000 °C. In fact, this would also explain why so far there are no other reports of low thermal stability of GeV: optical studies of the thermal stability of color centers in diamond rarely cover the low annealing temperature range, because in that regime the optical activation is also limited; therefore, such studies are performed in a regime where only reaction (1) is effective, and thus yield the high thermal stability associated with it.

Attempts have been reported [64] to increase the formation yield of GeV by means of irradiating Ge-implanted diamond with He ions, a process that creates additional vacancies but also interstitials. However, while it cannot be ruled out that this might initially increase the amount of GeV centers, the problem remains that a subsequent annealing step, which is required to achieve the optical properties, most likely converts the majority of them to substitutional Ge<sub>s</sub>. Recently, encouraging results were published regarding the enhancement of optical properties of GeV centers, in particular optical excitation power to reach saturation emission, created by means of ion implantation and high-pressure-high-temperature processing (HPHT, 15 min at 2000 °C and 6 GPa) [65]. However, this study did not assess the efficiency of formation of the optically active GeV<sup>-</sup> centers.

Last but not least, we would like to speculate what kind of processes are responsible for optical activation of implanted split-vacancy color centers, as we do not believe that the diffusion of vacancies during annealing is required to trigger their structural formation. In that respect, there are hardly any reports in the literature where optical activity of color centers from implanted impurities has been found at comparably low annealing temperatures. Unfortunately, this seems to not have been systematically investigated. In the case of Ge, [8] specifically reports the absence of the GeV<sup>-</sup> ZPL in the as-implanted state, but observation after annealing at 800 °C. The authors of [23] implanted Sn ions at an energy of 1 keV, resulting in an implantation depth of only around 20 Å. Following cleaning with H<sub>2</sub> plasma, the implanted layer was then overgrown by 900 Å of CVD diamond. This procedure resulted in the creation of SnV<sup>-</sup> centers with excellent optical properties, which was attributed by the authors to the H<sub>2</sub> plasma treatment and CVD overgrowth removing unwanted sp<sup>2</sup>-bonded carbon that may have resulted from implantation damage. However, it must be pointed out that due to CVD overgrowth occurring at 650 °C, the samples were implicitly also annealed,

although at a relatively low temperature, in comparison, e.g. to  $\sim 1100$  °C– $1200$  °C or above that is often used to activate  $\text{SnV}^-$  [22, 24–27]. To our knowledge, only one study claimed optical activity from implanted color centers *without any thermal annealing*. In a recent conference contribution [66], it was reported that, without any annealing, optical activation of a part of the implanted Mg impurities is possible simply by means of prolonged exposure to laser light in the 520–405 nm range (most efficiently blue 405 nm) before performing the actual PL experiment. This observation strongly suggests that a modification of the electronic environment contributes to the optical activation of implanted  $\text{MgV}^-$ . This is also intuitively suggested, taking into consideration that certain Fermi level conditions need to be met, e.g., for centers to be negatively charged, and interactions with photons of suitable energy can change the charge state of defects. In semiconductors where a wide variety of defects in a multitude of structural configurations are being introduced, e.g., through heavy irradiation, the Fermi level moves from its original position to a specific location (usually in the band gap) that can be predicted based only on the band structure of the semiconductor [67]. For diamond, this band gap pinning in the heavily damaged state is predicted to occur at 2.0–2.1 eV above the valence band [67], hence somewhat below midgap. Thermal annealing that removes defects, but also other treatments like surface functionalization or illumination with photons, can then change the position of the Fermi level. The importance of establishing suitable Fermi levels in order to increase optical activation is also outlined by other studies. For instance, it was reported that in B-doped diamond  $\sim 90\%$  of implanted Si atoms can be prepared optically active in the neutral state  $\text{SiV}^0$  [68]. Fermi-level engineering was also applied in [24, 25], where the authors reported enhanced optical activation of  $\text{SnV}^-$  (up to 8.6%) and  $\text{MgV}^-$  (up to 48.4%) following implantation into P-doped diamond. While the highest optical activation was achieved following annealing at  $1200$  °C, already at the lower annealing temperature of  $800$  °C a roughly threefold increase of optical activation was observed in comparison to undoped diamond. We hence suggest, that optical activation requires adjusting the structural and electronic environment of the split-vacancy complexes so that they a) exist in the desired charge state and b) are not perturbed by other defects nearby that could cause a major line shift or quench luminescence entirely.

## 5. Conclusions and outlook

GeV centers in split-vacancy configuration are created in sizable amounts ( $\sim 20\%$  of the implanted atoms) already during RT implantation, although at lower levels compared to other impurities, e.g. Sn [30], Mg [31] or Ga. Annealing or implanting at moderate temperatures ( $300$  °C) already significantly reduces the amount of GeV centers, reaching less than 10% at a temperature of  $900$  °C, accompanied by an increase in substitutional Ge. This behavior strongly suggests that the GeV complex in diamond is less thermally stable than simple substitutional Ge, as was predicted already by theory [32, 39], and we propose capture reactions with mobile carbon interstitials  $\text{C}_i$  to be responsible for the transformation to substitutional  $\text{Ge}_s$ . Also, contrary to NV for which thermal annealing favors the formation of optically active centers by enhancing both the structural formation yield and the optical activation, for GeV centers the effect of thermal annealing seems to be a competition between the detrimental effect of their structural depletion and the favorable annealing of other defects that allows for luminescence to be excited and observed.

The stability of split-vacancy vs substitutional configuration for group-IV impurities predicted in [32] correlates with the atomic size of the impurity, which is also intuitively expected. In that respect, it is not surprising that, in comparison to Sn, Ge to a larger extent prefers the substitutional position since this is what is predicted by theory. The theoretical predictions then further suggest that this would be even more so for the smaller Si atom. At the moment, however, it cannot be said whether Si presents a behavior that does not follow the expected trend. While *optically active*  $\text{SiV}^-$  seems to be an abundant defect in diamond, the *structural* formation yield of SiV following ion implantation has not been investigated so far. We note that in order for the group-IV vacancy centers to be optically active in their negative charge states, the Fermi level in diamond must be above the  $(0/-1)$  transition of the respective center, which scales with its atomic number, being lowest in the band gap for Si and highest for Pb [32, 34, 35, 37, 42]. It may thus be possible that the required Fermi-level conditions for  $\text{SiV}^-$  are easier to achieve than for the other impurities. In the future, we plan to address the case of Si in a similar manner as for Ge, by implanting the precursor isotope  $^{31}\text{Al}$  (644 ms) which decays into  $^{31}\text{Si}$  (157 min) and should allow to monitor the structural stability of the SiV configuration.

In future experiments we also intend to explore the formation yield of GeV for implantation below room temperature, which should further clarify the influence of temperature on its production mechanism. However, while this might increase the formation yield of the split-vacancy configuration (which already is higher at RT compared to  $300$  °C), the results presented here make it unlikely that large amounts of GeV will survive the annealing temperature step that is required to remove the implantation damage. A further goal will be to explore possible increases or decreases in GeV concentrations during post-implantation irradiation



with other (non-radioactive) ions easily available at ISOLDE during the same beam time, for the purpose of creating additional vacancies, e.g.,  $^{69}\text{Ga}$  or  $^{71}\text{Ga}$ . Characteristic differences in the behavior of Ga and Ge shall be further addressed in more detail by studying the lattice location of the short-lived  $^{76}\text{Ga}$  (32.6 s) isotope as function of implantation temperature in the whole temperature range up to 800 °C.

Further EC studies should also investigate possible differences in structural formation yield in diamonds which are doped with B acceptors or P donors, through a mechanism that locally modifies the Fermi level. As was already mentioned, doping with P donors was reported as beneficial for the optically active formation yield of  $\text{SnV}^-$  and  $\text{MgV}^-$ , supposedly due to a shift in Fermi level that causes vacancies to be negatively charged and thus prevents the formation of  $\text{V}_2$  or higher-order vacancy complexes, which compete with the formation of split-vacancy color centers [24, 25].











## Data availability statement

The data that support the findings of this study are openly available at the following URL/DOI: <https://doi.org/10.5281/zenodo.10091577>.

## Acknowledgments

We appreciate the support of the ISOLDE Collaboration and technical teams. This work was funded by the Portuguese Foundation for Science and Technology (Fundação para a Ciência e a Tecnologia FCT, CERN/FIS-TEC/0003/2021 UID/Multi/04349/2019, BD/11398/2022, UIDB/50011/2020 (DOI [10.54499/UIDB/50011/2020](https://doi.org/10.54499/UIDB/50011/2020)), UIDP/50011/2020 (DOI [10.54499/UIDP/50011/2020](https://doi.org/10.54499/UIDP/50011/2020)), LA/P/0006/2020 (DOI [10.54499/LA/P/0006/2020](https://doi.org/10.54499/LA/P/0006/2020))) from the Fonds voor Wetenschappelijk Onderzoek, Vlaanderen (FWO, Flanders), and from the KU Leuven (IBOF/23/065). The EU Horizon Europe Framework supported ISOLDE beam times through Grant Agreement 101057511 (EURO-LABS).

## ORCID iDs

Ulrich Wahl  <https://orcid.org/0000-0001-7398-2904>  
João Guilherme Correia  <https://orcid.org/0000-0002-8848-0824>  
Ângelo Costa  <https://orcid.org/0000-0002-9318-2418>  
Afonso Lamelas  <https://orcid.org/0000-0002-1668-6399>  
Vítor Amaral  <https://orcid.org/0000-0003-3359-7133>  
Karl Johnston  <https://orcid.org/0000-0002-0513-6869>  
Goele Magchies  <https://orcid.org/0000-0003-3186-4883>  
Shandirai Malven Tunhuma  <https://orcid.org/0000-0001-7423-9661>  
André Vantomme  <https://orcid.org/0000-0001-9158-6534>  
Lino M C Pereira  <https://orcid.org/0000-0002-1426-9102>

## References

- [1] Bradac C, Gao W, Forneris J, Trusheim M E and Aharonovich I 2019 Quantum nanophotonics with group IV defects in diamond *Nat. Commun.* **10** 5625
- [2] Chen D, Zheludev N and Gao W-B 2019 Building blocks for quantum network based on group-IV split-vacancy centers in diamond *Adv. Quantum Technol.* **3** 1900069
- [3] Wan N H et al 2020 Large-scale integration of artificial atoms in hybrid photonic circuits *Nature* **583** 226–31
- [4] Iwasaki T 2020 Color centers based on heavy group-IV elements *Semicond. Semimetals* **103** 237–56
- [5] Ruf M, Wan N H, Choi H, Englund D and Hanson R 2021 Quantum networks based on color centers in diamond *J. Appl. Phys.* **130** 070901
- [6] Becher C et al 2023 2023 roadmap for materials for quantum technologies *Mater. Quantum Technol.* **3** 012501
- [7] Nguyen C T et al 2019 An integrated nanophotonic quantum register based on silicon-vacancy spins in diamond *Phys. Rev. B* **100** 165428
- [8] Iwasaki T et al 2015 Germanium-vacancy single color centers in diamond *Sci. Rep.* **5** 12882
- [9] Palyanov Y N, Kupriyanov I N, Borzdov Y M and Surovtsev N V 2015 Germanium: a new catalyst for diamond synthesis and a new optically active impurity in diamond *Sci. Rep.* **5** 14789
- [10] Ekimov E A, Lyapin S G, Boldyrev K N, Kondrin M V, Khmelitskiy R, Gavva V A, Kotereva T V and Popova M N 2015 Germanium–vacancy color center in isotopically enriched diamonds synthesized at high pressures *JETP Lett.* **102** 701–6
- [11] Zhou Y, Mu Z, Adamo G, Bauerdick S, Rudzinski A, Aharonovich I and Gao W B 2018 Direct writing of single germanium vacancy center arrays in diamond *New J. Phys.* **20** 125004
- [12] Evans R E, Sipahigil A, Sukachev D D, Zibrov A S and Lukin M D 2016 Narrow-linewidth homogeneous optical emitters in diamond nanostructures via silicon ion implantation *Phys. Rev. Appl.* **5** 04410
- [13] Lagomarsino S et al 2018 Optical properties of silicon-vacancy color centers in diamond created by ion implantation and post-annealing *Diam. Relat. Mater.* **84** 196–203
- [14] Lagomarsino S et al 2021 Creation of silicon-vacancy color centers in diamond by ion implantation *Front. Phys.* **8** 601362

- [15] Hunold L, Lagomarsino S, Flatae A M, Kambalathmana H, Sledz F, Sciortino S, Gelli N, Giuntini L and Agio M 2021 Scalable creation of deep silicon-vacancy color centers in diamond by ion implantation through a 1- $\mu\text{m}$  pinhole *Adv. Quantum Technol.* **4** 2100079
- [16] Sipahigil A et al 2016 An integrated diamond nanophotonics platform for quantum-optical networks *Science* **354** 847–50
- [17] Schröder T et al 2017 Scalable focused ion beam creation of nearly lifetime-limited single quantum emitters in diamond nanostructures *Nat. Commun.* **8** 15376
- [18] ES B, Abraham J B S and DL P 2019 Optimization of SiV defect yield in diamond substrates *Sandia Technical Report SAND-2016-9436R* (Sandia National Lab. (SNL-NM)) (<https://doi.org/10.2172/1562424>)
- [19] Titze M, Byeon H, Flores A, Henshaw J, CT H, Mounce A M and Bielejec E S 2022 In situ ion counting for improved implanted ion error rate and silicon vacancy yield uncertainty *Nano Lett.* **22** 3212–8
- [20] Marseglia L et al 2018 Bright nanowire single photon source based on SiV centers in diamond *Opt. Express* **26** 80–89
- [21] Tamura S et al 2014 Array of bright silicon-vacancy centers in diamond fabricated by low-energy focused ion beam implantation *Appl. Phys. Express* **7** 115201
- [22] Rugar A E, Dory C, Sun S and Vučković J 2019 Characterization of optical and spin properties of single tin-vacancy centers in diamond nanopillars *Phys. Rev. B* **99** 205417
- [23] Rugar A E, Lu H, Dory C, Sun S, McQuade P J, Shen Z X, Melosh N A and Vučković J 2020 Generation of tin-vacancy centers in diamond via shallow ion implantation and subsequent diamond overgrowth *Nano Lett.* **20** 1614–9
- [24] Lühmann T, John R, Wunderlich R, Meijer J and Pezzagna S 2019 Coulomb-driven single defect engineering for scalable qubits and spin sensors in diamond *Nat. Commun.* **10** 4956
- [25] Lühmann T, Meijer J and Pezzagna S 2021 Charge-assisted engineering of color centers in diamond *Phys. Status Solidi a* **218** 2000614
- [26] Iwasaki T, Miyamoto Y, Taniguchi T, Siyushev P, Metsch M H, Jelezko F and Hatano M 2017 Tin-vacancy quantum emitters in diamond *Phys. Rev. Lett.* **119** 253601
- [27] Ditalia Tchernij S et al 2017 Single-photon-emitting optical centers in diamond fabricated upon Sn implantation *ACS Photonics* **4** 2580–6
- [28] Trusheim M E et al 2020 Transform-limited photons from a coherent tin-vacancy spin in diamond *Phys. Rev. Lett.* **124** 023602
- [29] Frösch J E et al 2020 Versatile direct-writing of dopants in a solid state host through recoil implantation *Nat. Commun.* **11** 5039
- [30] Wahl U, Correia J G, Villarreal R, Bourgeois E, Gulka M, Nesladek M, Vantomme A and Pereira L M C 2020 Direct structural identification and quantification of the split-vacancy configuration for implanted Sn in diamond *Phys. Rev. Lett.* **125** 045301
- [31] Corte E et al 2023 Magnesium-vacancy optical centers in diamond *ACS Photonics* **10** 101–10
- [32] Goss J P, Briddon P R, Rayson M J, Sque S J and Jones R 2005 Vacancy-impurity complexes and limitations for implantation doping of diamond *Phys. Rev. B* **72** 035214
- [33] Komarovskikh A, Dmitriev A, Nadolinny V and Palyanov Y 2017 A DFT calculation of EPR parameters of a germanium-vacancy defect in diamond *Diam. Relat. Mater.* **76** 86–89
- [34] Häußler S et al 2017 Photoluminescence excitation spectroscopy of SiV<sup>-</sup> and GeV<sup>-</sup> color center in diamond *New J. Phys.* **19** 063036
- [35] Thiering G and Gali A 2018 *Ab initio* magneto-optical spectrum of group-IV vacancy color centers in diamond *Phys. Rev. X* **8** 021063
- [36] Boldyrev K N, Mavrin B N, Sherin P S and Popova M N 2018 Bright luminescence of diamonds with Ge-V centers *J. Lumin.* **193** 119–24
- [37] Defo R K, Kaxiras E and Richardson S L 2019 How carbon vacancies can affect the properties of group IV color centers in diamond: a study of thermodynamics and kinetics *J. Appl. Phys.* **126** 195103
- [38] Thiering G and Gali A 2019 The ( $e_g \otimes e_u$ )  $\otimes E_g$  product Jahn–Teller effect in the neutral group-IV vacancy quantum bits in diamond *npj Comput. Mater.* **5** 18
- [39] Krivobok V S, Ekimov E A, Lyapin S G, Nikolaev S N, Skakov Y A, Razgulov A A and Kondrin M V 2020 Observation of a 1.979-eV spectral line of a germanium-related color center in microdiamonds and nanodiamonds *Phys. Rev. B* **101** 144103
- [40] Ciccario C J, Flick J, Harris I B, Trusheim M E, Englund D R and Narang P 2020 Strong spin–orbit quenching via the product Jahn–Teller effect in neutral group IV qubits in diamond *npj Quantum Mater.* **5** 75
- [41] Boldyrev K N, Sedov V S, Vanpoucke D E P, Ralchenko V G and Mavrin B N 2022 Localized vibrational modes of GeV-centers in diamond: photoluminescence and first-principles phonon study *Diam. Relat. Mater.* **126** 109049
- [42] Qiu C, Deng H X, Geng S and Wei S H 2023 Origin of structure and zero-phonon-line anomalies of XV centers in diamond (X=Si, Ge, Sn, Pb) *Phys. Rev. B* **107** 214110
- [43] Brewer L 1975 Cohesive energies of the elements *Technical Report 3720* (Lawrence Berkeley National Lab. (LBNL)) (<https://doi.org/10.2172/7187973>)
- [44] Koike J, Parkin D M and Mitchell T E 1992 Displacement threshold energy for type IIa diamond *Appl. Phys. Lett.* **60** 1450–2
- [45] Ziegler J F, Ziegler M D and Biersack J P 2010 SRIM—the stopping and range of ions in matter (2010) *Nucl. Instrum. Methods Phys. Res. B* **268** 1818–23
- [46] Hofsäss H and Lindner G 1991 Emission channeling and blocking *Phys. Rep.* **201** 121–83
- [47] Wahl U 2000 Advances in electron emission channeling measurements in semiconductors *Hyperfine Interact.* **129** 349–70
- [48] Wahl U et al 2004 Position-sensitive Si pad detectors for electron emission channeling experiments *Nucl. Instrum. Methods Phys. Res. A* **524** 245–56
- [49] Silva M R, Wahl U, Correia J G, Amorim L M and Pereira L M C 2013 A versatile apparatus for on-line emission channeling experiments *Rev. Sci. Instrum.* **84** 073506
- [50] Catherall R et al 2017 The ISOLDE facility *J. Phys. G: Nucl. Part. Phys.* **44** 094002
- [51] Fedosseev V, Chrysalidis K, Day Goodacre T, Marsh B, Rothe S, Seiffert C and Wendt K 2017 Ion beam production and study of radioactive isotopes with the laser ion source at ISOLDE *J. Phys. G: Nucl. Part. Phys.* **44** 084006
- [52] Supplementary material to “Structural formation yield of GeV centers from implanted Ge in diamond”
- [53] David-Bosne E, Wahl U, Correia J G, Lima T A L, Vantomme A and Pereira L M C 2020 A generalized fitting tool for analysis of two-dimensional channeling patterns *Nucl. Instrum. Methods Phys. Res. B* **462** 102–13
- [54] Agostinelli S et al 2003 (GEANT4 Collaboration) 2003 GEANT4—A simulation toolkit *Nucl. Instrum. Methods Phys. Res. A* **506** 250–303
- [55] Wahl U et al EC-SLI Collaboration 2024 Beta emission channeling patterns from <sup>75</sup>Ge and <sup>75</sup>Ga in diamond *Zenodo* (<https://doi.org/10.5281/zenodo.10091577>)

- [56] Goss J P, Lowery R, Briddon P R and Rayson M J 2024 Density functional theory study of Al, Ga and In impurities in diamond *Diam. Relat. Mater.* **142** 110811
- [57] Harris I, Ciccarino C J, Flick J, Englund D R and Narang P 2020 Group-III quantum defects in diamond are stable spin-1 color centers *Phys. Rev. B* **102** 195206
- [58] Christinck J, Hirt F, Hofer H, Liu Z, Eitzkorn M, Dunatov T, Jakšić M, Forneris J and Kück S 2023 Bright single-photon emission from a GeV center in diamond under a microfabricated solid immersion lens at room temperature *J. Appl. Phys.* **133** 193102
- [59] Davies G, Lawson S C, Collins A T, Mainwood A and Sharp S J 1992 Vacancy-related centers in diamond *Phys. Rev. B* **46** 13157–70
- [60] Newton M E, Campbell B A, Twitchen D J, Baker J M and Anthony T R 2002 Recombination-enhanced diffusion of self-interstitial atoms and vacancy-interstitial recombination in diamond *Diam. Relat. Mater.* **11** 618–22
- [61] Allers L, Collins A T and Hiscock J 1998 The annealing of interstitial-related optical centres in type II natural diamond *Diam. Relat. Mater.* **7** 228–32
- [62] Twitchen D J, Hunt D C, Wade C, Newton M E, Baker J M, Anthony T R and Banholzer W F 1999 The production and annealing stages of the self-interstitial (R2) defect in diamond *Physica B* **273–274** 644–46
- [63] Jakubovskii K, Kiflawi I, Johnston K, Collins A, Davies G and Stesmans A 2003 Annealing of vacancies and interstitials in diamond *Physica B* **340–342** 67–75
- [64] Chakraborty T, Sankaran K J, Srinivasu K, Nongjai R, Asokan K, Chen C H, Niu H and Haenen K 2021 Enhancement of concentration of XeV and GeV centers in microcrystalline diamond films through He<sup>+</sup> irradiation *Diam. Relat. Mater.* **120** 108587
- [65] Nieto Hernández E *et al* 2023 Efficiency Optimization of Ge-V quantum emitters in single-crystal diamond upon ion implantation and HPHT annealing *Adv. Quantum Technol.* **6** 2300010
- [66] Nieto Hernández E, Pugliese V, Corte E, Ditalia Tchernij S, Olivero P and Forneris J 2024 CW laser activation of color centers in diamond *Hasselt Diamond Workshop SBDD XXVIII*
- [67] Brudnyi V, Grinyaev S N and Stepanov V E 1995 Local neutrality concept: fermi level pinning in defective semiconductors *Physica B* **212** 429–35
- [68] Rose B C *et al* 2018 Observation of an environmentally insensitive solid-state spin defect in diamond *Science* **361** 60–63